

UKAEA-CCFE-PR(18)17

J. D. T. Allen, A. Mottura and A. Breidi

First-Principles Modeling of the Temperature Dependence for the Superlattice Intrinsic Stacking Fault Energies in $L1_2$ Ni_{75-x} X_x Al_{25} Alloys

Enquiries about copyright and reproduction should in the first instance be addressed to the UKAEA Publications Officer, Culham Science Centre, Building K1/0/83 Abingdon, Oxfordshire, OX14 3DB, UK. The United Kingdom Atomic Energy Authority is the copyright holder.

First-Principles Modeling of the Temperature Dependence for the Superlattice Intrinsic Stacking Fault Energies in L1₂ Ni_{75-x}X_x Al_{25} Alloys

J. D. T. Allen,¹ A. Mottura¹ and A. Breidi²

¹*School of Metallurgy and Materials, University of Birmingham, Edgbaston B15 2TT, United Kingdom*

²*UK Atomic Energy Authority, Culham Science Centre, Oxfordshire OX14 3DB, UK*

1 **First-principles modeling of the temperature dependence for the**
2 **superlattice intrinsic stacking fault energies in $L1_2$ $Ni_{75-x}X_xAl_{25}$**
3 **alloys**

4 J. D. T. Allen and A. Mottura

5 *School of Metallurgy and Materials, University of Birmingham,*
6 *Edgbaston B15 2TT, United Kingdom*

7 A. Breidi*

8 *UK Atomic Energy Authority, Culham Science Centre, Oxfordshire OX14 3DB, UK*

9 (Dated: May 29, 2018)

10 **Abstract**

11 Stronger and more resistant alloys are required in order to increase the performance and efficiency
12 of jet engines and gas turbines. This will eventually require planar faults engineering, or a complete
13 understanding of the effects of composition and temperature on the various planar faults that
14 arise as a result of shearing of the γ' precipitates. In this work, a combined scheme consisting
15 of the density functional theory, the quasi-harmonic Debye model, and the axial Ising model, in
16 conjunction with a quasistatic approach are used to assess the effect of composition and temperature
17 of a series of pseudo-binary alloys based on the $(Ni_{75-x}X_x)Al_{25}$ system using distinct relaxation
18 schemes to assess observed differences. Our calculations reveal that the (111) superlattice intrinsic
19 stacking fault energies in these systems decline modestly with temperature between 0 K and 1000 K.

20 I. INTRODUCTION

21 In precipitation-strengthened alloys, the shearing of particles is often one of the active
22 deformation mechanisms. Superalloys are no exception to this, and their complex shearing
23 mechanisms are indeed partly responsible for their superior mechanical properties at high
24 temperatures. Over the last few decades, increasing focus has been spent on understanding
25 these shearing mechanisms, which change with composition and temperature. The crystal
26 structure of the matrix (γ , fcc) and precipitate (γ' , L1₂) phase is such that a full dislocation
27 in the matrix results in the introduction of an anti-phase boundary (APB) in the precipitate
28 phase. Other partial dislocations can also shear these precipitates, leading to a diverse range
29 of faults: superlattice intrinsic stacking faults (SISFs), superlattice extrinsic stacking faults
30 (SESFs), complex stacking faults (CSFs), which can themselves be intrinsic or extrinsic,
31 twin structures and more complicated planar defects.

32 The energies of these planar faults are extremely important as they determine the nature
33 of the complex dislocation structures shearing the precipitates, as well as the segregation of
34 solute elements to the fault energies, which in turns can affect the motion of dislocations
35 through the precipitates. As a result, a number of mechanical properties, such as minimum
36 grain size due to milling, strain hardening and yield stress depend on planar fault ener-
37 gies. Creep resistance is also affected by the planar fault energies¹. As microstructure and
38 processing methods are refined further, it may be possible to achieve even higher strengths
39 and high-temperature properties through planar faults engineering. Therefore, a complete
40 understanding of the effect of composition and temperature on planar fault energies must
41 be developed in order to exploit these opportunities.

42 Planar fault energies can be measured experimentally, by determining the separation
43 between partials using transmission electron microscopes. However, the thin-film effects
44 and uncertainty about how to apply relevant corrections make this type of experimental
45 work very difficult²⁻⁴. These issues also make it very difficult to systematically study the
46 effect of composition and temperature on these planar fault energies.

47 On the other hand, recent experimental work has shown robust evidence of solute seg-
48regation to these planar faults in the superalloys, often referred to as Suzuki segregation⁵.
49 Several studies have successfully employed scanning transmission electron microscopy, often
50 coupled with energy dispersive spectroscopy, to map solute concentration at SISFs, SESFs

51 and twin structures in both Ni- and Co-based superalloys^{6,7}. At the same time, the density
 52 functional theory (DFT) has been employed to compute relevant planar fault energies, and
 53 to assess the effect of composition on these values. Two main approaches exist for calculating
 54 planar fault energies using the DFT. A more traditional approach involves calculating the
 55 energy differences between a perfect and a faulted supercell, thereby simulating the planar
 56 fault explicitly^{8,9}. An alternative approach is to employ the Ising model to describe the
 57 energy of a large supercell as a sum of contributions arising from the interactions of pairs
 58 of planes¹⁰. Both methods have been used to compute various planar fault energies and the
 59 effect of composition on planar fault energies for γ' - Ni₃Al-based alloys^{8,9,11}.

60 One of the main limitations of the available theoretical studies is that all values are
 61 computed at 0 K. This may be a problem since the superalloys are usually operating at
 62 appreciable temperatures. Thus, it becomes necessary to assess how these energies may
 63 change as temperature is increased. In our recent major work¹¹, we have established the
 64 effect of composition on the SISF energies in all γ' - Ni₃Al-based alloys at 0 K. We have
 65 as well addressed the temperature effect on the SISF energies for several Ni₃Al-based sys-
 66 tems, specifically: $(Ni_{75-x}Co_x)Al_{25}$, $(Ni_{75-x}Cu_x)Al_{25}$, $(Ni_{75-x}Pd_x)Al_{25}$, $(Ni_{75-x}Pt_x)Al_{25}$.
 67 However, our temperature-dependence results (section IV.B.3¹¹) are preliminary, since they
 68 did not involve local atomic relaxations of the D0₁₉ structure. Thereby, the SISF energies
 69 temperature-dependence presented earlier¹¹ was tentative. In this work, we try to establish
 70 the SISF energies variation as a function of temperature. The investigated alloys are those
 71 recently¹¹ addressed: $(Ni_{75-x}X_x)Al_{25}$ pseudo-binary system, where $X = \text{Co, Cu, Pd or Pt}$,
 72 and $x = 4.62975, 9.2595, 13.88925$ and 18.51825 at. % X. We employ a combined scheme con-
 73 sisting of DFT, the quasi-harmonic Debye (QHD) model, and the axial Ising model (AIM),
 74 in conjunction with a quasistatic approach. Furthermore, we assess the effect of relaxations
 75 on the overall results by applying two distinct schemes: full internal relaxation where atoms
 76 within the structure are allowed to relax to their lowest energy position, and internally static
 77 whereby the positions of atoms are kept fixed within the structures.

81 II. COMPUTATIONAL METHOD

82 We combine DFT calculations with the AIM and the QHD model in order determine
 83 the temperature dependence of SISF energies in L1₂ Ni₃Al-based alloys. This paper does

84 not focus on the methodology behind both models, nor on their advantages/disadvantages
 85 relative to other approaches (Supercell method and phonon calculations). However, we will
 86 adequately introduce the main formalisms of both AIM and QHD models that helped us to
 87 have direct access into SISF energies and their thermal dependence. For more details, the
 88 reader is referred to Refs. 11 and 12 and references therein.

89 **A. AIM model**

90 We employ the axial nearest-neighbor Ising model (ANNI) which is the first-order ap-
 91 proximation of the AIM model. The (111) SISF formation energy of L1₂ alloys using the
 92 ANNI model is given by:

$$93 \quad \gamma_{\text{ANNI}}^{L1_2} = \frac{8(E_{D0_{19}} - E_{L1_2})}{V_{L1_2}^{2/3} \cdot \sqrt{3}}, \quad (1)$$

94 where V_{L1_2} is the volume of 4-atoms L1₂ unit cell and $V_{L1_2}^{2/3} \cdot \sqrt{3}$ is the area of 4-atoms in the
 95 L1₂ (111) plane over which the stacking fault extends. E_{L1_2} and $E_{D0_{19}}$ are the energies per
 96 atom of the L1₂ and D0₁₉ structures.

97 **B. QHD model**

98 The QHD model is able to establish the equation of state of a solid, *i.e.*, the volume
 99 temperature-dependence $V=f(T)$ where V is the equilibrium volume at a given temperature
 100 T . This is achieved through minimizing the non-equilibrium Gibbs function as:

$$101 \quad \left(\frac{\partial G^*}{\partial V} \right)_{T,P} = 0, \quad (2)$$

102 where

$$103 \quad G^*(T, P, V) = E_e(V) + PV + A_{vib}(T, V). \quad (3)$$

104 E_e is the total energy of the system at a given volume V , calculated using the DFT. P is
 105 the ambient pressure, $A_{vib}(T, V)$ is the Helmholtz vibrational energy term. This term is the
 106 core-element of the model as it consists of an approximation of the vibrational density of
 107 states (DOS) known as Debye's phonon DOS. The minimization of G^* is implemented in
 108 the **gibbs** code¹³.

109 Let's mention here that the computational method presented here was used recently¹¹ to

110 calculate a preliminary temperature-dependence of SISF energies in L1₂ Ni₃Al-based alloys,
 111 with the exception that in this study we take into account the local atomic relaxations
 112 of the D0₁₉ phase, which makes the approach more robust and complete in establishing
 113 qualitatively and quantitatively the desired thermal dependence.

114 C. Supercell modeling and first-principles techniques

115 The Ni_{75-x}X_xAl₂₅ alloy was modeled using 108-atom L1₂-based 3×3×3(×4-atoms) and
 116 216-atom D0₁₉-based 3×3×3(×8-atoms) supercells. The transition metal ternary element X
 117 (Co,Cu,Pd,Pt) occupy exclusively the Ni-sites as the latter manifest strong site-preference
 118 to the Ni-sublattice¹⁴⁻¹⁷. In our study, the alloy compositions fall within the experimen-
 119 tal solubility of X in Ni₃Al alloys¹⁴. The used supercells were generated to satisfy the
 120 chemical disorder on the Ni-sublattice where the Warren-Cowley short-range order (SRO)
 121 parameters^{18,19} were minimized at several nearest neighbor coordination shells.

122 The first-principles calculations were performed using the Density-functional theory DFT^{20,21}
 123 as implemented in the Vienna Ab initio Simulation Package (VASP)²²⁻²⁴, which employs
 124 the Projector Augmented Wave PAW method to determine the total energies and forces.
 125 The exchange-correlation (XC) energy of electrons is described in the generalized gradient
 126 approximation (GGA) using the functional parameterization of Perdew-Burke-Ernzerhof²⁵.
 127 The energy cut-off was set to 400 eV. A mesh of a 112 and 63 special **k**-points for 108-
 128 Atom L1₂ and 216-Atom D0₁₉ phases, respectively, were taken in the irreducible wedge of
 129 the Brillouin zone for the total energy calculations. These input parameters stabilized the
 130 energy differences between L1₂ and D0₁₉ phases and guaranteed the uncertainty in SISF
 131 energy to be less than 2 mJ/m².

132 During relaxation of the L1₂ phase, the supercell shape was kept fixed. Only volume and
 133 atomic positions were allowed to change in order to fully minimize the total energy. This
 134 technique prevents the L1₂ supercell from deviating to a low symmetric phase.

135 Concerning the D0₁₉ phase, only local atomic relaxations were allowed. The D0₁₉ volume-
 136 per-atom was intentionally set to the corresponding L1₂ equilibrium value, while the *c/a*
 137 ratio was kept constant at the D0₁₉ ideal value. This insured that $a_{D0_{19}}$ and $c_{D0_{19}}$ corre-
 138 spond to the underlying L1₂ lattice, *i.e.*, $a_{D0_{19}}/a_{L1_2} = \sqrt{2}$ and $c_{D0_{19}}/a_{L1_2} = \sqrt{4/3}$. For
 139 both phases, the local atomic relaxations were carried out using the conjugate gradient

140 algorithm²⁶, a powerful scheme commonly used to relax the atoms into their instantaneous
141 ground state.

142 III. RESULTS

143 The (111) SISF energy temperature dependence in L1₂ Ni₃Al-based alloys is calculated
144 through a combined DFT-AIM-QHD approach. Let us mention here that this approach
145 is quasistatic since the temperature-dependence of the SISF energy is obtained through a
146 DFT calculation of the of L1₂ and D0₁₉ energies at a volume V corresponding to a sought-
147 after temperature T . Hence, it becomes clear now that this approach assumes that the
148 temperature-dependence of SISF energies is attributed only to thermal expansion *i.e.*, other
149 thermal effects, namely, electronic, vibrational and magnetic thermal excitations are not
150 accounted for.

151 The SISF energy temperature-dependence is realized by firstly feeding the **gibbs** code¹³ a
152 set of L1₂ Energy-Volume values being determined with VASP code as demonstrated above.
153 **gibbs** will search for an equilibrium volume that minimizes the non-equilibrium Gibbs energy
154 at a given temperature, hence volume temperature-dependence of lattice L1₂ is established.
155 Then, upon selecting a desired temperature T , we simulate the D0₁₉ energy with VASP at
156 the corresponding equilibrium volume. Finally, the SISF energy corresponding to a temper-
157 ature T is evaluated using the AIM model as expressed by Eq. 1

158 Several experimental reports^{27–29} back this quasistatic approach. It has been shown to be
159 effective in calculating the elastic constants of Ni₃Al^{30,31}. It has been as well shown to
160 be successful when calculating the elastic constants of Ta³² where thermal expansivity was
161 the dominant temperature contribution, while other thermal effects such as phonon and
162 electronic excitation contributions were found to be quite minor at constant volume. Of
163 particular importance to this study is the recent success in applying this approach to calcu-
164 late the SISF energies in unaries³³, pure compounds¹² and alloys³⁴ characterized by complex
165 magnetic structures.

166 Figs. 1, 2, 3 and 4 present the SISF energy temperature dependence of the L1₂ Ni_{75-x}Co_xAl₂₅,
167 Ni_{75-x}Cu_xAl₂₅, Ni_{75-x}Pd_xAl₂₅ and Ni_{75-x}Pt_xAl₂₅ alloys, respectively. Some of the compo-
168 sitions studied, taking into account the volume relaxation only (*i.e.*, with atomic positions
169 fixed, as in the left panels of Figs. 1-4), have been preliminarily reported by us¹¹. The

170 first thing to notice upon analyzing the results is the significant reduction in SISF ener-
 171 gies upon performing local atomic relaxations observed in all compositions and systems.
 172 It is worth mentioning at this point that the values predicted with local-atomic-relaxation
 173 scheme should be more close to the experimental values. The magnitude of the reduction
 174 varies significantly between the studied systems and across the alloying compositions. The
 175 reduction is highly pronounced in $\text{Ni}_{75-x}\text{Pd}_x\text{Al}_{25}$ and $\text{Ni}_{75-x}\text{Pt}_x\text{Al}_{25}$, and less pronounced
 176 in $\text{Ni}_{75-x}\text{Co}_x\text{Al}_{25}$ and $\text{Ni}_{75-x}\text{Cu}_x\text{Al}_{25}$. For the sake of comparison, consider the composition
 177 13.88925 at. %. Given this composition, the average difference (across temperature) between
 178 volume and local-atomic-relaxation schemes reaches a value as large as 138 mJ/m^2 when
 179 substituting Ni by Pt, to be compared with 26 mJ/m^2 when substituting Ni by Cu.
 180 The drop in the calculated SISF energies due to inclusion of atomic relaxations can be ex-
 181 plained in terms of the size-argument *i.e.*, the atomic-radius mismatch. If we consider the
 182 system $\text{Ni}_{75-x}\text{Pt}_x\text{Al}_{25}$, Pt atoms characterized by large Wigner-Seitz (WS) radii (1.5319 \AA)
 183 are substituting small Ni atoms ($\text{WS}=1.3756 \text{ \AA}$) and this atomic-size mismatch is responsi-
 184 ble for important atomic relaxations leading the system into its lowest energy configuration
 185 which is very much different from that of fixed-atomic-positions calculations. While, Cu
 186 characterized by $\text{WS}=1.4107 \text{ \AA}$ which is not much larger than Ni ($\text{WS}=1.3756 \text{ \AA}$), hence
 187 the effect of local-atomic-relaxations is less pronounced in comparison with systems having
 188 Pt and Pd (1.52 \AA) as alloying elements. We need to emphasize here that we have derived
 189 the equilibrium Wigner-Seitz radii (WS) from the room temperature (R.T.) experimental
 190 atomic volumes³⁵ ($V_{exp}^{RT} = \frac{4}{3}\pi WS^3$) of the alloying element ground state structure.
 191 On the other hand, the variation of the local-atomic-relaxation SISF energies upon increas-
 192 ing temperature exhibits a small linear decrease relative to 0 K values for the whole studied
 193 compositions. The magnitude of this decrease barely reaches 10 mJ/m^2 at its maximum.
 194 In fact, in our previous investigation¹¹ we have shown that the change in SISF energies as
 195 a function of alloying compositions, upon allowing local-atomic-relaxations, for the solutes
 196 Co, Cu, Pd and Pt is not significant, which is in contrast to the large increase induced by
 197 solutes substituting for Al sites. Consequently, it follows from the results presented here and
 198 Ref.¹¹ that both alloying and temperature effects have little impact on changing the SISF
 199 energies in $\text{Ni}_{75-x}\text{X}_x\text{Al}_{25}$ alloys.

200 IV. CONCLUSIONS

201 A combined computational scheme consisting of DFT, QHD and AIM in conjunction with
202 a quasistatic approach enabled us to establish the temperature-dependence of SISF energies
203 in $L1_2$ $Ni_{75-x}X_xAl_{25}$ alloys. We find that a proper relaxation of both $L1_2$ and $D0_{19}$ phases
204 is indispensable to predict a reliable estimation of the SISF energies. Our results, without
205 an exception, all display a linear decline of the SISF energies as a function of composition.
206 Interestingly, this decline is very modest, in average it is less than 10 mJ/m^2 (SISF value
207 at 1000 K relative to 0 K). This insignificant decrease in SISF energies and consequently
208 the minor effect of temperature on the 0 K value is motivating, as it reduces drastically
209 the computational cost required to calculate the SISF energies at every single temperature.
210 Hence, it seems plausible to consider the 0 K SISF energy of a $L1_2$ multicomponent alloy
211 $(Ni,Cu,Pd,Pt)_{75}Al_{25}$ valid to use in physics-based deformation models³⁶ needed to predict
212 primary creep of Ni-superalloys at their operating temperature. We assert that this conclu-
213 sion is only valid for alloying elements substituting for Ni-sites, and therefore can not be
214 extended to include elements substituting for Al-sites. We also emphasize that our SISF
215 energy temperature-dependence is based on volume expansion as the only thermal effect.

216 V. ACKNOWLEDGEMENTS

217 This study made use of these computational facilities: (a) University of Birmingham's
218 BlueBEAR HPC service (<http://www.birmingham.ac.uk/bear>), (b) MidPlus Regional HPC
219 Center (www.hpc-midlands-plus.ac.uk), and (c) Beskow cluster ([https://www.pdc.kth.se/hpc-](https://www.pdc.kth.se/hpc-services/computing-systems/beskow-1.737436)
220 [services/computing-systems/beskow-1.737436](https://www.pdc.kth.se/hpc-services/computing-systems/beskow-1.737436)), we are therefore very much grateful and
221 would like to thank them for making this work possible. We would like, as well, to ac-
222 knowledge the EPSRC (grant EP/M021874/1) and EU FP7 (grant GA109937) for financial
223 support. Part of this work (A. Breidi) has been carried out within the framework of the
224 EUROfusion Consortium and has received funding from the Euratom research and training
225 programme 2014-2018 under grant agreement No 633053 and from the RCUK Energy Pro-
226 gramme [grant number EP/P012450/1]. The views and opinions expressed herein do not

227 necessarily reflect those of the European Commission.

228 * corresponding author; a.breidi@hotmail.com

229 ¹ C. Rae and R. Reed, *Acta Materialia* **55**, 1067 (2007).

230 ² L. V. and J. O. Nilsson and B. Johansson, *Acta Materialia* **54**, 3821 (2006).

231 ³ Y. Qi and R. K. Mishra, *Physical Review B* **75**, 224105 (2007).

232 ⁴ C. B. Carter and S. M. Holmes, *The Philosophical Magazine* **35**, 1161 (1977).

233 ⁵ H. Suzuki, *Journal of the Physical Society of Japan* **17**, 322 (1962).

234 ⁶ V. Vorontsov, L. Kovarik, M. Mills, and C. Rae, *Acta Materialia* **60**, 4866 (2012).

235 ⁷ G. Viswanathan, R. Shi, A. Genc, V. Vorontsov, L. Kovarik, C. Rae, and M. Mills, *Scripta*
236 *Materialia* **94**, 5 (2015).

237 ⁸ N. Eurich and P. Bristowe, *Scripta Materialia* **102**, 87 (2015).

238 ⁹ K. V. Vamsi and S. Karthikeyan, in *Superalloys 2012* (John Wiley & Sons, Inc., 2012) pp.
239 521–530.

240 ¹⁰ P. J. H. Denteneer and W. van Haeringen, *Journal of Physics C: Solid State Physics* **20**, L883
241 (1987).

242 ¹¹ A. Breidi, J. Allen, and A. Mottura, *Acta Materialia* **145**, 97 (2018).

243 ¹² A. Breidi, J. Allen, and A. Mottura, *physica status solidi (b)* **254**, n/a (2017).

244 ¹³ M. Blanco, E. Francisco, and V. Luaña, *Computer Physics Communications* **158**, 57 (2004).

245 ¹⁴ Y. Mishima, S. Ochiai, and T. Suzuki, *Acta Metallurgica* **33**, 1161 (1985).

246 ¹⁵ A. V. Ruban, V. Popov, V. Portnoi, and V. Bogdanov, *Philosophical Magazine* **94**, 20 (2014).

247 ¹⁶ C. Jiang and B. Gleeson, *Scripta Materialia* **55**, 433 (2006).

248 ¹⁷ A. V. Ruban and H. L. Skriver, *Phys. Rev. B* **55**, 856 (1997).

249 ¹⁸ J. M. Cowley, *Journal of Applied Physics* **21**, 24 (1950).

250 ¹⁹ B. Warren, *X-ray diffraction* (New York, Dover, 1990).

251 ²⁰ P. Hohenberg and W. Kohn, *Phys. Rev.* **136**, B864 (1964).

252 ²¹ W. Kohn and L. J. Sham, *Phys. Rev.* **140**, A1133 (1965).

253 ²² G. Kresse and D. Joubert, *Phys. Rev. B* **59**, 1758 (1999).

254 ²³ G. Kresse and J. Furthmüller, *Computational Materials Science* **6**, 15 (1996).

255 ²⁴ P. E. Blöchl, *Phys. Rev. B* **50**, 17953 (1994).

- 256 ²⁵ J. P. Perdew, K. Burke, and M. Ernzerhof, Phys. Rev. Lett. **77**, 3865 (1996).
- 257 ²⁶ W. Press, S. Teukolsky, W. Vetterling, and B. Flannery, (Cambridge University Press, 2007).
- 258 ²⁷ C. Swenson, Journal of Physics and Chemistry of Solids **29**, 1337 (1968).
- 259 ²⁸ E. Wasserman, in *Handbook of Ferromagnetic Materials*, Handbook of Ferromagnetic Materials,
260 Vol. 5 (Elsevier, 1990) pp. 237 – 322.
- 261 ²⁹ O. L. Anderson and D. G. Isaak, “Elastic constants of mantle minerals at high temperature,” in
262 *Mineral Physics & Crystallography: A Handbook of Physical Constants* (American Geophysical
263 Union, 2013) pp. 64–97.
- 264 ³⁰ Y. Wang, J. J. Wang, H. Zhang, V. R. Manga, S. L. Shang, L.-Q. Chen, and Z.-K. Liu, Journal
265 of Physics: Condensed Matter **22**, 225404 (2010).
- 266 ³¹ S.-L. Shang, H. Zhang, Y. Wang, and Z.-K. Liu, Journal of Physics: Condensed Matter **22**,
267 375403 (2010).
- 268 ³² O. Gülseren and R. E. Cohen, Phys. Rev. B **65**, 064103 (2002).
- 269 ³³ I. Bleskov, T. Hickel, J. Neugebauer, and A. Ruban, Phys. Rev. B **93**, 214115 (2016).
- 270 ³⁴ V. I. Razumovskiy, A. Reyes-Huamantínco, P. Puschnig, and A. V. Ruban, Phys. Rev. B **93**,
271 054111 (2016).
- 272 ³⁵ C. Kittel, *Introduction to Solid State Physics*, 7th ed. (Wiley, New York, 1996, 1996).
- 273 ³⁶ Y.-K. Kim, D. Kim, H.-K. Kim, C.-S. Oh, and B.-J. Lee, International Journal of Plasticity
274 **79**, 153 (2016).

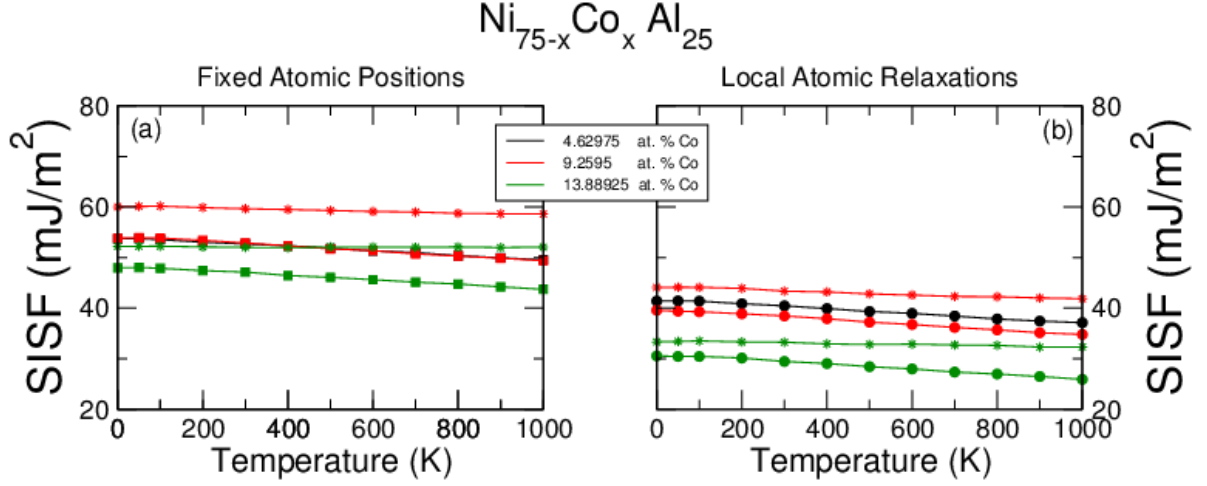


FIG. 1. Variation of the SISF energies as a function of temperature for the System $L1_2$ $\text{Ni}_{75-x}\text{Co}_x\text{Al}_{25}$. The star symbols designate spin-polarized calculations. In panel (a) the data corresponding to the composition 4.62975 at.% Co are not visible because they are extremely close to those of 9.2595 at.% Co. The lines going through the data are purely for visual reasons.

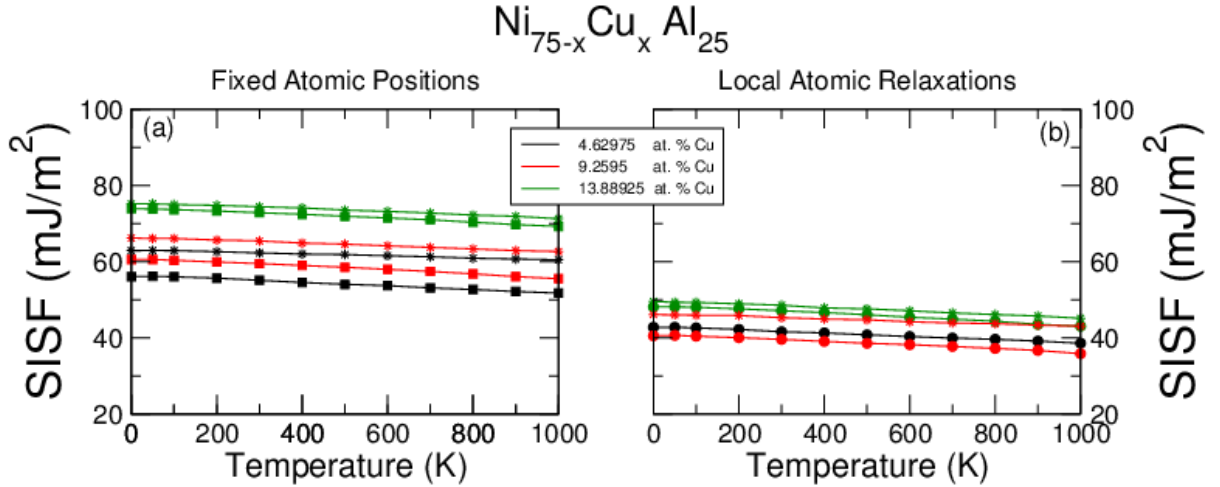


FIG. 2. Change of SISF energies upon temperature increase in the system $L1_2$ $\text{Ni}_{75-x}\text{Cu}_x\text{Al}_{25}$. The star symbols designate spin-polarized calculations. The lines going through the data are purely for visual reasons.

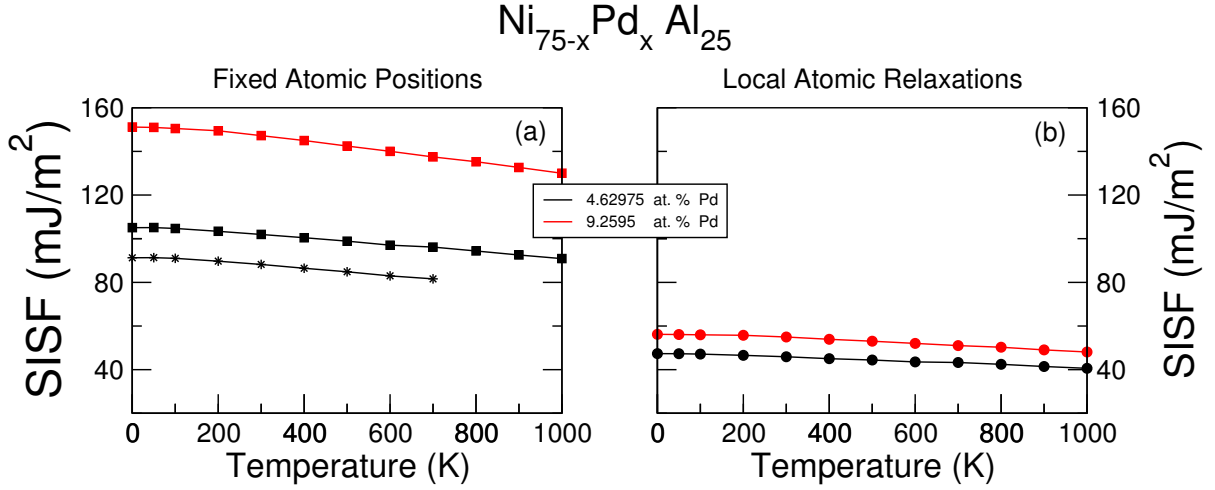


FIG. 3. Temperature dependence of SISF energies in $L1_2 \text{Ni}_{75-x}\text{Pd}_x\text{Al}_{25}$. The star symbols indicate spin-polarized calculations. The lines connecting the points are only to help guiding the eyes through the data.

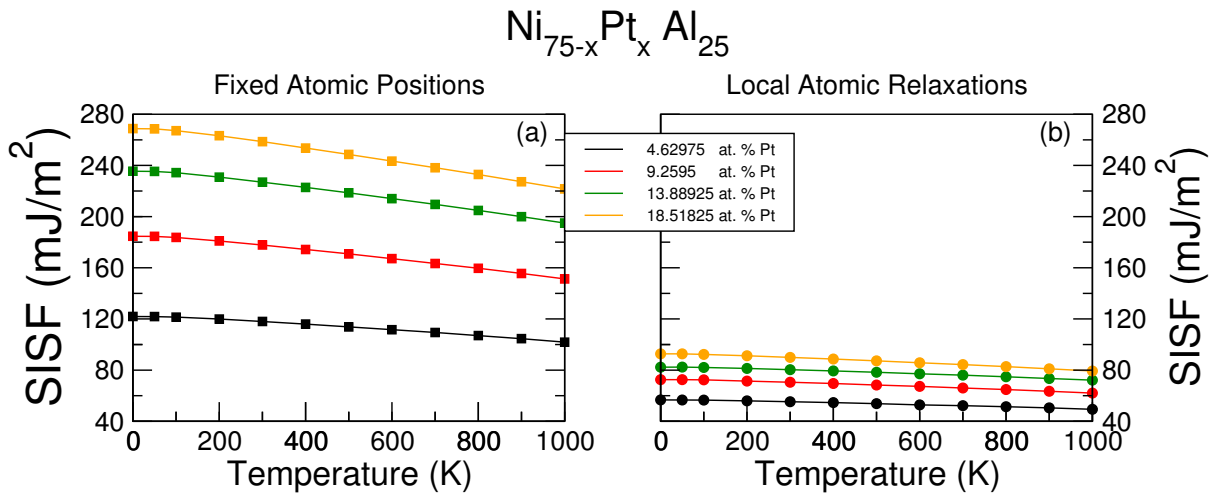


FIG. 4. Temperature dependence of SISF energies in $L1_2 \text{Ni}_{75-x}\text{Pt}_x\text{Al}_{25}$. The lines connecting the points are only to help guiding the eyes through the data.